Super-virtual refraction interferometry: an engineering field data example

Sherif M. Hanafy[1,2*] and Ola Al-Hagan[1]

[1] *King Abdullah University of Science and Technology (KAUST), Physical Science and Engineering Division, Thuwal 23955-6900, Saudi Arabia*

[2] *On leave from Geophysics Dept. Faculty of Science, Cairo University, Giza, Egypt*

ABSTRACT

The theory of super-virtual refraction interferometry (SVI) was recently developed to enhance the signal-to-noise ratio (SNR) of far-offset traces in refraction surveys. This enhancement of the SNR is proportional to $\sqrt{N}$ and can be as high as N if an iterative procedure is used. Here N is the number of post-critical shot positions that coincides with the receiver locations. We now demonstrate the SNR enhancement of super-virtual refraction traces for one engineering-scale synthetic data and two field seismic data sets. The field data are collected over a normal fault in Saudi Arabia. Results show that both the SNR of the super-virtual data set and the number of reliable first-arrival traveltime picks are significantly increased.

INTRODUCTION

Refraction traveltime tomography is used to find the detailed structure of near-surface geology (Zhu *et al.* 1992; Higuera-Diaz *et al.* 2007; Hanafy 2010), as well as to image the gross crustal velocity structure of the earth (Mooney and Weaver 1989; Zelt and Smith 1992; Sheriff and Geldart 1995; Funck *et al.* 2008). A significant problem with current refraction surveys is that they require stronger sources in order to record first arrivals with a high signal-to-noise ratio (SNR) at far-offset traces. Without a sufficiently high SNR in far-offset traces the refraction traveltimes cannot be accurately picked. To partly overcome this problem, Dong *et al.* (2006) and later Bharadwaj and Schuster (2010) developed the theory of refraction interferometry to increase the SNR of head-wave arrivals. As shown in Fig. 1(a), the Dong *et al.* (2006) method correlates a pair of traces to give the correlation trace $\phi_x(\mathbf{A},\mathbf{B}, t)$, where $\mathbf{A}$ and $\mathbf{B}$ are the geophone positions and $\mathbf{x}$ is the source position. The right-hand side of Fig. 1(a) illustrates that the resulting virtual trace will have a virtual refraction arrival with an arrival time of $\tau_{A'B}$ - $\tau_{A'A}$. Repeating this procedure for any post-critical source position in the figure will lead to a virtual trace with the same virtual refraction traveltime, so stacking correlated traces $\Sigma_x \phi_x(\mathbf{A},\mathbf{B}, t)$ over all post-critical source positions will yield a trace containing a virtual refraction event with an enhanced SNR. This enhancement is proportional to $\sqrt{N}$, where N is the number of sources that generates this particular head wave. Dong *et al.* (2006) demonstrated this method on land data over a salt dome in central Utah and later Nichols *et al.* (2010) dem-

onstrated its effectiveness over a hydrogeophysical research site in Idaho.

A problem with refraction interferometry is that, if only the head-wave arrivals are correlated with one another, the virtual head-wave trace has the correct moveout pattern but will not arrive at the actual propagation time. The virtual refraction has an unknown excitation time, so as a remedy, Dong *et al.* (2006) suggested that the source be virtually relocated to the surface by calibrating the virtual stacked refraction trace to an observed traveltime in the raw data. Another problem is that the correlation of traces typically decreases the source-receiver offset of the virtual trace because traveltimes are subtracted and are associated with shorter raypaths (Schuster 2009). To overcome these problems Bharadwaj and Schuster (2010), Mallinson *et al.* (2011) and Bharadwaj *et al.* (2011) presented an extension of refraction interferometry so that the receiver spread could be extended to its maximum recording extent and the absolute arrival time is properly accounted for. This new method creates far-offset refraction arrivals by a combination of both correlation (Fig. 1a) and convolution (Fig. 1b) of traces with one another to create what is denoted as super-virtual refraction traces. Mallinson *et al.* (2011) presented the work flow for super-virtual refraction interferometry (SVI) and demonstrated its effectiveness with both synthetic and field data results but only gave an intuitive explanation of its underlying principles. Later, Bharadwaj and Schuster (2012) and Bharadwaj *et al.* (2011) presented the rigorous theory of SVI.

In this paper, SVI will be implemented on engineering-scale seismic data to enhance the SNR of far-offset traces. The first
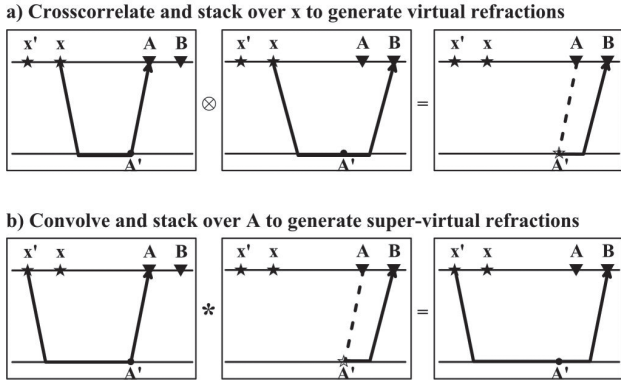
*sherif.geo@gmail.com

a) Crosscorrelate and stack over x to generate virtual refractions

b) Convolve and stack over A to generate super-virtual refractions

FIGURE 1

The steps for creating super-virtual refraction arrivals. a) Correlation of the recorded trace at **A** with that at **B** for a source at x to give the trace $\phi_x(\mathbf{A},\mathbf{B}, t)$ with the virtual refraction having traveltime denoted by $\tau_{A'B}$ - $\tau_{A'A}$. This arrival time will be the same for all post-critical source positions, so stacking $\Sigma_x\phi_x(\mathbf{A},\mathbf{B}, t)$ will enhance the SNR of the virtual refraction by $\sqrt{N}$. b) Similar to that in a) except the virtual refraction traces are convolved with the actual refraction traces and stacked for different geophone positions to give the super-virtual trace with a SNR enhanced by $\sqrt{N}$. Here, N denotes the number of coincident source and receiver positions that are at post-critical offset for this particular refraction.

part of this paper presents a summary of the SVI theory. This is followed by synthetic and field data examples that show the benefits and limitations of using this method and finally the last section presents a summary.

THEORY

The SVI method was described by Bharadwaj and Schuster (2010), Bharadwaj and Schuster (2012), Bharadwaj *et al*. (2011) and Mallinson *et al*. (2011). They used the far-field reciprocity equation of both correlation (equation (1)) and convolution (equation (2)) types to create super-virtual refractions and enhance the SNR by a factor of $\sqrt{N}$, where N is the number of source positions (coincident with receiver) associated with the generation of the head-wave arrival.

$$Im\left[G(\mathbf{A}|\mathbf{B})^{virt.}\right] \approx\sim k \int_{post-crit\,sources} G(\mathbf{A}|\mathrm{x})^* G(\mathbf{B}|\mathrm{x})dx \qquad (1)$$

$$G(\mathbf{B}|\mathrm{x}')^{super} \approx 2ik \int_{receivers} G(\mathbf{A}|\mathbf{B})^{virt.} G(A|\mathrm{x}')dA \qquad (2)$$

where the source positions are at **x** in Fig. 1(a) and **x**′ in Fig. 1(b), the receivers are at **A** and **B**, k is the average wavenumber, $G(\mathbf{A}|\mathbf{B})$ represents the head-wave contribution in the Green's function for a virtual shot at **A**′, a receiver at **B** and the virtual excitation time is equal to the negative traveltime from **A** to **A**′. $G(\mathbf{B}|\mathrm{x}')^{super}$ denotes the super-virtual data obtained by convolving the recorded data $G(\mathbf{A}|\mathrm{x}')$ with the virtual data $G(\mathbf{A}|\mathbf{B})^{virt.}$ (Fig. 1b).

To avoid artefacts due to the integration over a limited recording aperture and discrete sampling, Dong *et al*. (2006) suggested
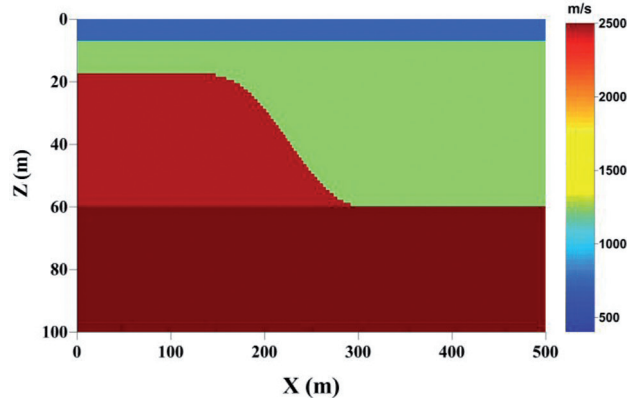

FIGURE 2

Velocity model used to generate the synthetic data. The source wavelet is a Ricker wavelet with a peak frequency of 40 Hz. The 160 sources and receivers are placed on the surface and spaced at 3 m intervals.

windowing about the first arrivals so that only head-wave arrivals are correlated with one another.

The workflow of the SVI method is as follows:

1. Filter the raw data to remove high-frequency noise.
2. Window about the first arrivals; the suggested window length is 1 period before the expected first-arrival times and 2 to 3 periods after it.
3. Use equation (1) to generate the virtual traces.
4. Use equation (2) to generate the super-virtual traces.

One drawback of this method is, due to the limited recording aperture and coarse spacing of the sources and receivers, there may be some artefacts in the super-virtual data set. In this case, either a dip filter or a least-squares approach to the redatuming might be used to mitigate such noise. Another problem is that the long-offset refractions might have very high noise levels, which may degrade the quality of the final super-virtual refraction. A partial remedy is to exclude these traces and use only traces with less noise to create the final super-virtual traces.

SYNTHETIC EXAMPLE

The SVI method is tested on a synthetic data set generated by a finite-difference solution to the acoustic wave equation for the velocity model shown in Fig. 2. Here, there are 160 receiver and shot points located at the top of the model at 3 m intervals. The source wavelet is a Ricker wavelet peaked at 40 Hz. Random noise with a bandwidth of 10–50 Hz is added to the traces so that the refraction events are not clearly visible.

Figure 3(a) shows a sample shot gather after adding random noise and windowing about the first arrivals; the head-wave refractions are masked by the noise and the SNR is low for the far-offset traces. Figure 3(b) is the super-virtual shot gather after applying the interferometry method described in the previous section. The traces now have high SNR so the first-arrival times can be accurately picked. However, the source wavelet has
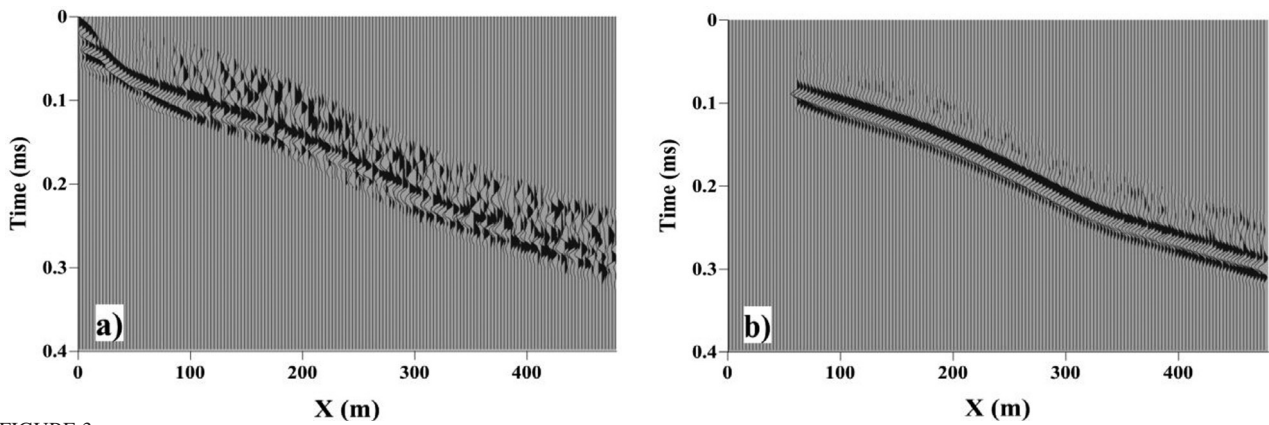
FIGURE 3

a) Synthetic CSG with a surface source located at 3 m after adding random noise to all traces. b) Super-virtual CSG with an improved SNR.
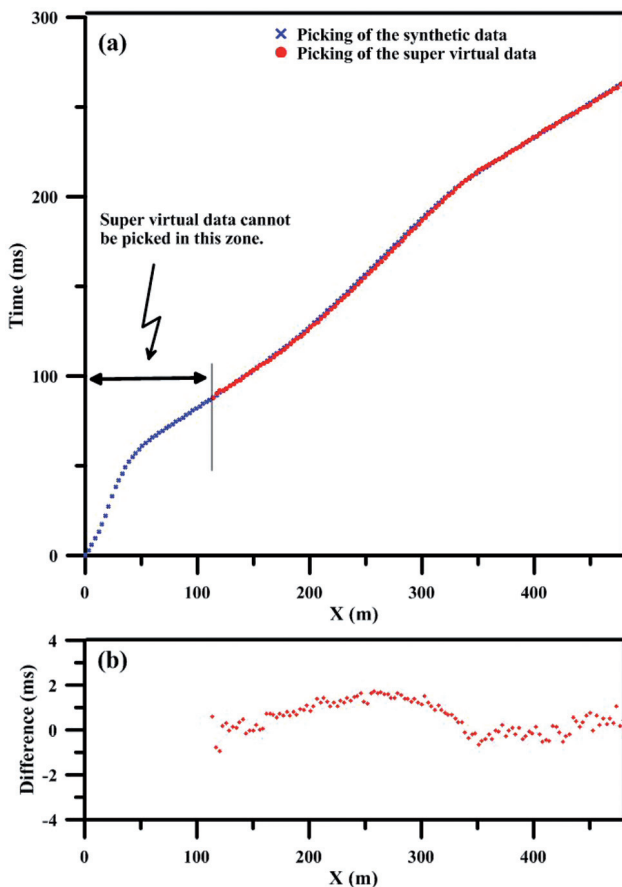

FIGURE 4

a) Comparison between the picked traveltimes for the raw traces and super-virtual traces for a synthetic CSG. b) The differences in traveltime picks.

FIGURE 5

Histogram comparing traveltime differences at traces where both raw and super-virtual traces can be picked.

broadened (Fig. 3b) due to the correlation of the traces with one another. If this presents a problem in resolution then a wavelet deconvolution filter can be applied to the data. Since the first arrivals are required for traveltime tomography, the accuracy of these picks should be checked by examining the traveltime differe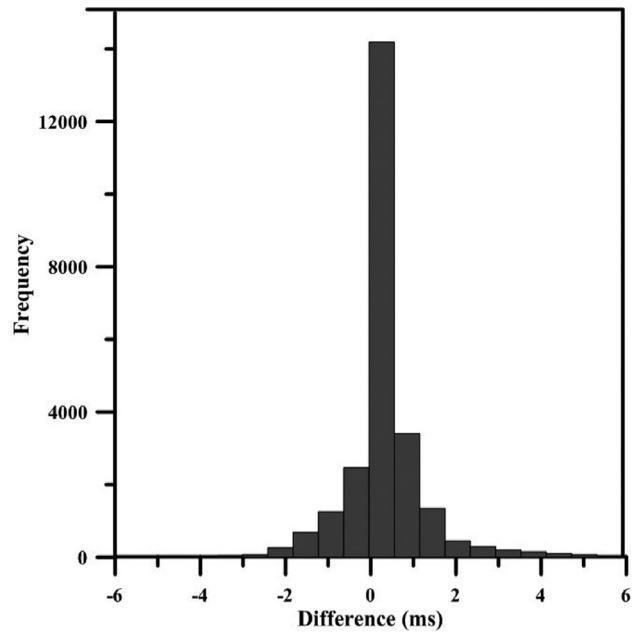nces between the super-virtual picks and the raw-data noise-free picks. Figure 4 shows a comparison between the first-arrival picks from the super-virtual gather and the noise-free raw data sets. The difference here is within T/4=6 ms, as shown in Fig. 4 where T is the wavelet period of the raw data. The histogram in Fig. 5 shows that 97% of the super-virtual picks are within a quarter of a period of the corresponding picks from the raw data.

FIELD DATA EXAMPLE

The proposed SVI method is tested using two field examples collected on the western region of Saudi Arabia, 90 km north of Jeddah. The first field data set has a high SNR, where the first arrivals can be accurately picked. The second field example is a noisy data set, where the first arrivals can be picked up to a
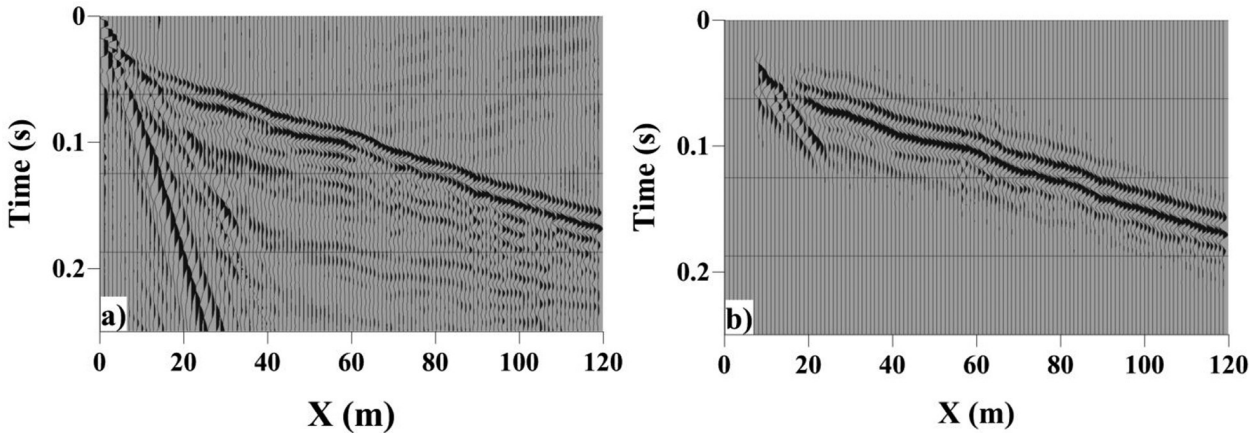
FIGURE 6

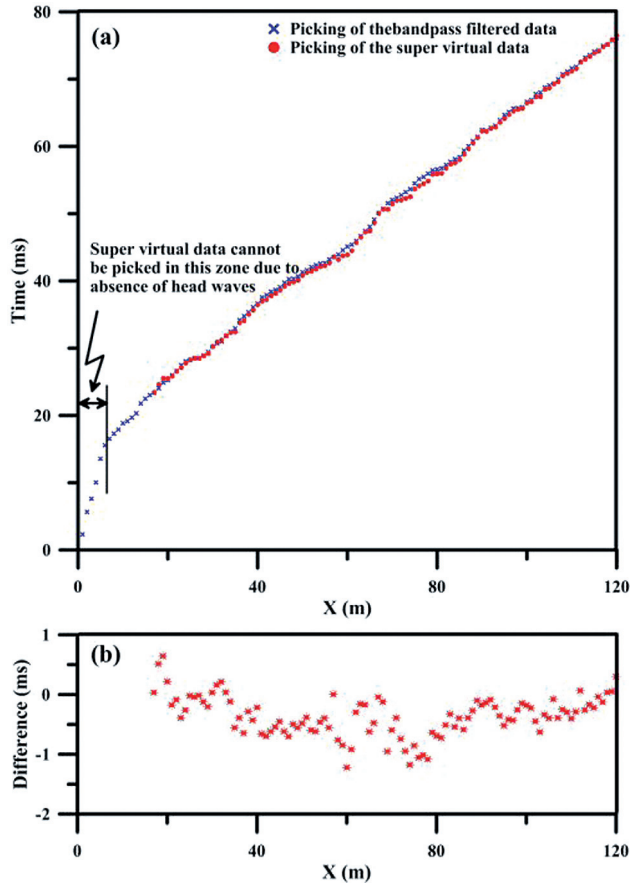a) A shot gather example of the clean field data set. b) Super-virtual shot gather.

FIGURE 7

a) Comparison between the picked traveltimes for the raw and super-virtual traces for the field data. b) The differences in traveltime picks.

source-receiver offset of 150 m and show a low SNR with unpickable first arrivals at larger source-receiver offsets. We used the clean field data set as a ground truth test to show that the proposed method will not significantly change the actual traveltimes, it will only increase the SNR.
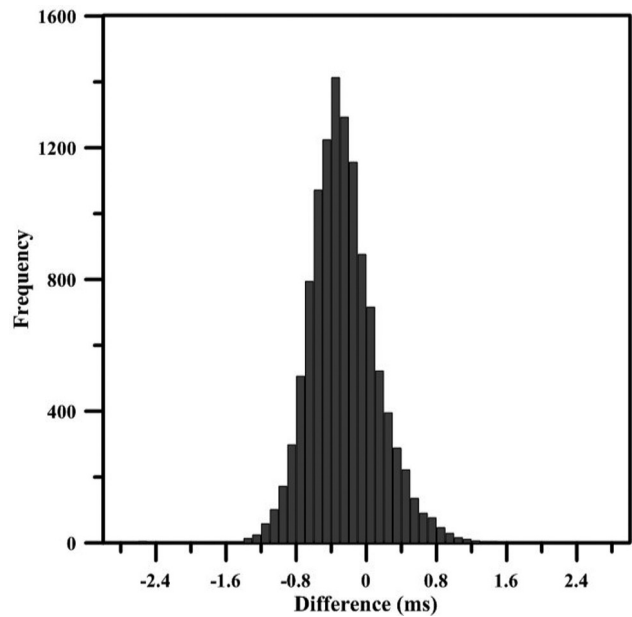

FIGURE 8

Histogram comparing traveltime differences at traces where both raw and super-virtual traces can be picked, the input data are the raw and SVI traveltime picks of the clean field example.

Field data example 1: clean data set

The field data were recorded by 120 receivers spaced at 1 m intervals and 120 shot points are located at the receiver locations. Figure 6(a) is a shot gather from the data and is characterized by a high SNR, here all first arrivals can be picked. The SVI method is applied to these traces to create super-virtual traces shown in Fig. 6(b). Comparing the raw and super-virtual shot gathers shows that there are no significant differences between their first-arrival traveltimes. To validate the accuracy of the proposed method, first-arrival times were picked in the super-virtual gathers and compared to the raw data picks in Fig. 7. The differences in these traveltimes are mostly within $T/4 = 6$ ms of each other
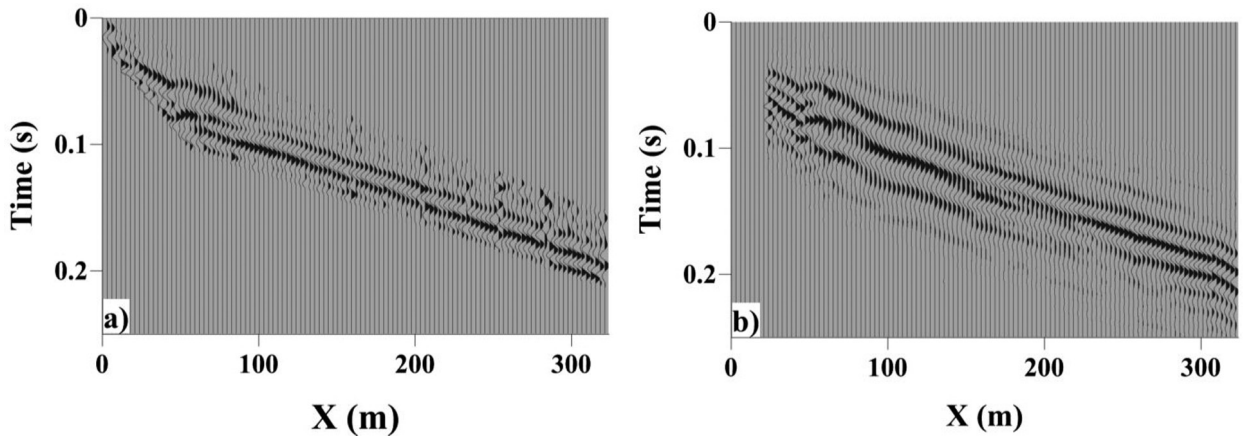
FIGURE 9

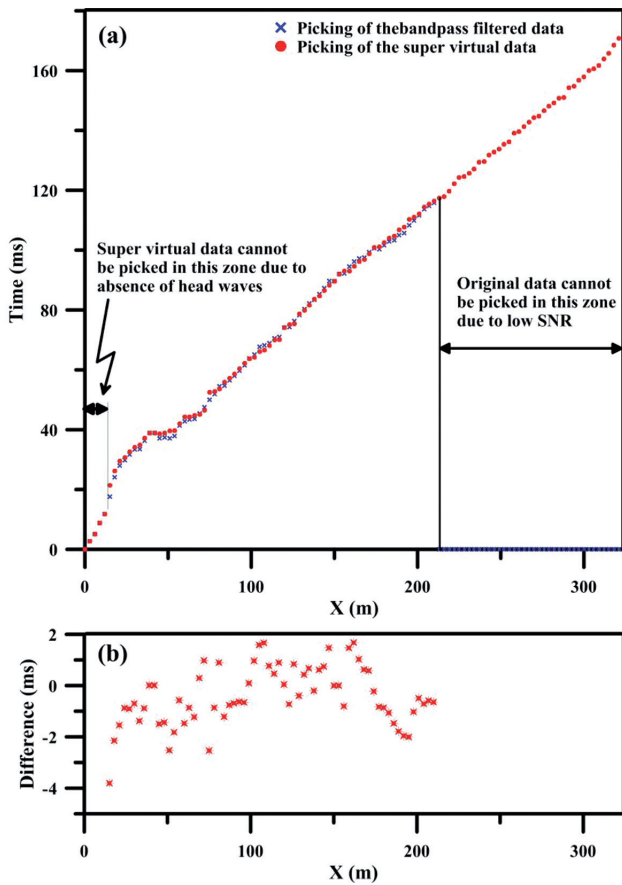a) Raw shot gather after band-pass filtering and b) the super-virtual CSG with an improved SNR.

FIGURE 10

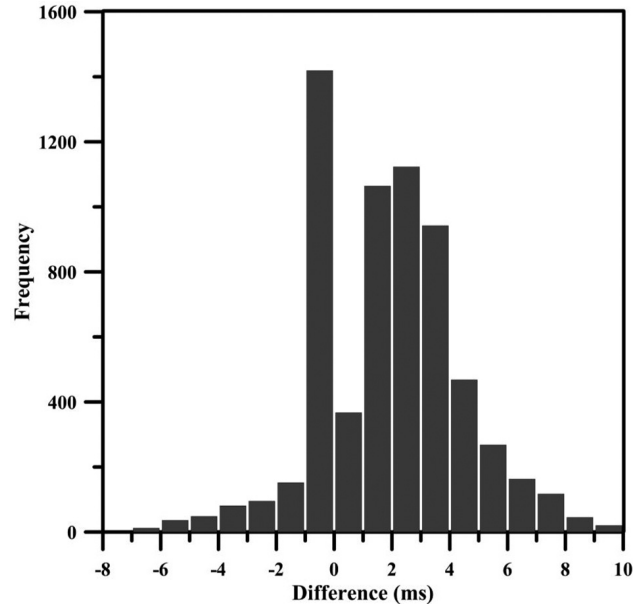Graphs comparing raw data and super-virtual data picks for one shot gather.

FIGURE 11

Histogram comparing traveltime differences at traces where both raw and super-virtual traces can be picked; the input data are the raw and SVI traveltime picks of the noisy field example.

Field data example 2: noisy data set

A refraction field data set is collected on the western side of Saudi Arabia along a known fault system. A total of 109 active receivers are used with receiver offsets of 3 m and a total of 109 shot gathers were collected with one shot located at each receiver location. The frequency spectrum of this data set shows a peak frequency of 40 Hz, so that a band-pass filter with a low cut of 5–10 Hz and a high pass of 100–120 Hz was used to remove high-frequency noise (Fig. 9a). In Fig. 9(a), far-offset traces show a low SNR and the first-arrival traveltimes cannot be picked.

To remedy this problem, the windowed traces are correlated and summed (see equation (1)) to create virtual traces and then convolv-

as shown in Fig. 7 for shot gather 1, where T is the wavelet period. Figure 8 shows the histogram of the differences between the picked times of the raw and the super-virtual traces, where over 98% of the picked traces have a traveltime difference less than $T/4 = 6$ ms.
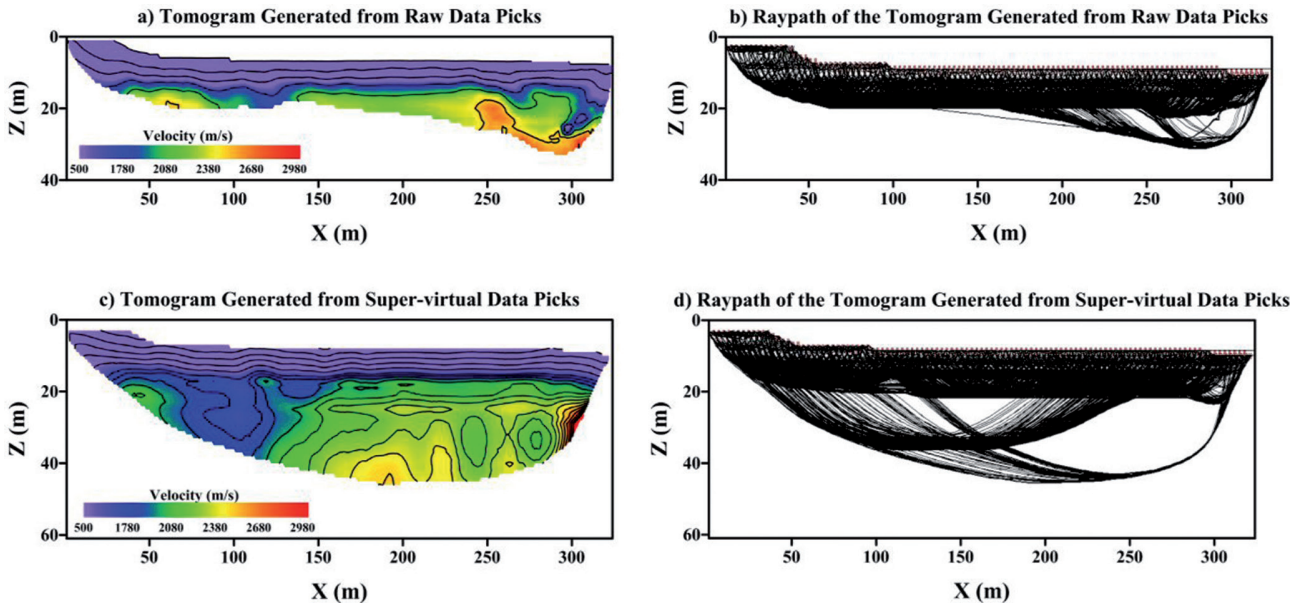
FIGURE 12

(a) Tomogram of the noisy field example using traveltime picks from raw data with a band-pass filter, (b) the corresponding raypath diagram.
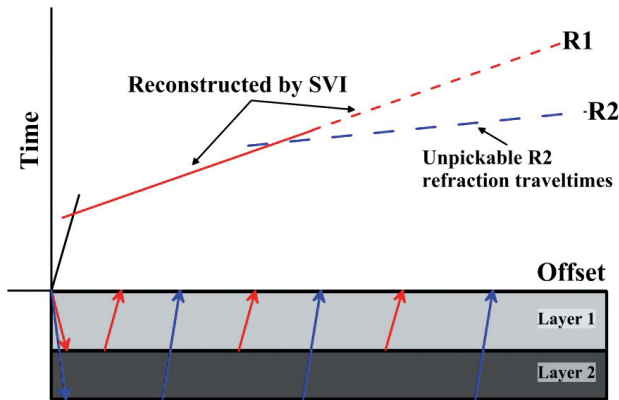(c) Tomogram of the same data set using SVI traveltime picks and (d) the corresponding raypath diagram.

FIGURE 13

First-arrival traveltimes curves for refractions from interfaces R1 and R2.

ing these virtual traces with the raw traces yields, after stacking (see equation (2)), the super-virtual traces shown in Fig. 9(b). It is clear that the first-arrival traveltimes can be picked in the super-virtual traces compared to the unpickable far-offset traces in Fig. 9(a).

To validate the accuracy of the picked traveltimes, Fig. 10 compares the first-arrival times picked in the super-virtual gather to the band-pass filtered data. The difference in these traveltimes is mostly within $T/4 = 6$ ms of each other for shot gather 1, where T is the wavelet period. Figure 11 shows the histogram of the traveltime difference between the picked times of the band-pass filtered and the super-virtual data sets; the histogram shows that over 90% of the picked traces have a difference less than $T/4 = 6$ ms.

The super-virtual traces are obtained by the correlation and convolution of the raw traces so that the source wavelet becomes ringy. This can lead to an ambiguous identification of the first arrival, which can create a consistent traveltime discrepancy with respect to the actual arrival time. This discrepancy can be eliminated if we find the average difference between the super-virtual traveltime and the actual traveltime picks for traces with a high SNR (near-offset traces) and then subtract this value from all super-virtual picks. Another possible solution is wavelet deconvolution.

To illustrate the importance of the far-offset first-arrival picks for traveltime tomography, Fig. 12(a,b) presents the tomogram of the first-arrival traveltimes of the band-pass filtered data set and the corresponding raypath diagram, respectively. The total number of picked traveltimes is 10250. To eliminate unreliable picks a reciprocity test[1] is made so that only accurate picks are included in the inversion process. A total of 762 picks did not pass the reciprocity test and only 9488 picks are included in the inversion. Most of the rejected picks are from far-offset shot-receiver pairs due to the low SNR at these traces. The maximum source-receiver offset in the accepted data is 240 m. The first-arrival traveltimes of the 11881 SVI traces are picked and then inverted (Fig. 12c). Here, 842 picks did not pass the reciprocity test and

---

1 If the difference between the first-arrival traveltime picks τ_{xy} and τ_{yx} is greater than a predefined threshold value, then both picks are rejected. Here, τ_{yx} is the traveltime pick for a shot located at x and receiver located at y, while τ_{yx} is the traveltime pick for a shot located at y and receiver located at x. The threshold value used here is $T=4 = 6$ ms, where T is the dominant period.

11039 picks are included in the inversion to generate the tomogram shown in Fig. 12(c). Since the SVI method increased the SNR of the far-offset traces, more far-offset picks are included in the SVI tomogram than the original data tomogram. The super-virtual tomogram shows a penetration depth of 53 m and provides new information about the subsurface. Note the near-offset raypaths in both the original data and the super-virtual tomograms are very similar to one another (Fig. 12b and Fig. 12d). Figure 12(d) shows far-offset raypaths (shots at $X = 0$–50 m with receivers at $X > 200$ m and shots at $X > 280$ m with receivers at $X = 0$–100 m), which gives a deeper depth of penetration compared to Fig. 12(b).

LIMITATIONS OF THE SVI METHOD

One limitation of the SVI method that needs to be emphasized is illustrated in Fig. 1, which shows the reconstruction of long-offset refractions (raypath **x´B**) from shorter-offset refractions (raypaths **xA** and **xB**). If the actual first arrival at either the intermediate or far offsets is damaged, then the reconstructed long-offset SVI events may not represent the actual first arrivals but instead are the later refraction arrivals from a shallow refractor. This problem can be worsened if the window about the first arrivals is incorrectly selected.

An example of this problem is shown in Fig. 13 where the dotted line represents the R2 refraction traveltimes, which are too damaged to be picked or reconstructed by the SVI method. Assuming that the shorter offset records do not contain the R2 refractions, then the SVI procedure is likely to only reconstruct the far-offset R1 traveltimes from the shorter-offset records. This assumes that these shorter offset records contain R1 refractions and the R2 refractions are too damaged. In this case, the long-offset SVI traces only contain R1 refractions records and so do not illuminate refractors below the R1 refractor.

CONCLUSIONS

Using the super-virtual refraction interferometry method, the signal-to-noise ratio (SNR) of far-offset head-wave arrivals can be theoretically increased by a factor $\sqrt{N}$, where N is the number of post-critical receiver positions vitiated by a source. Super-virtual refractions are generated in two steps, the first is the correlation of the traces with one another to generate traces with virtual head-wave arrivals and the second is convolution of the data with the virtual traces to create traces with super-virtual head-wave arrivals. This method is valid for any medium that generates head-wave arrivals at geophones and it will not significantly enhance the SNR of pure-diving waves.

The SVI method is tested on one synthetic and two field data sets. Results show that the SVI method enhances the SNR of far-offset traces so the first-arrival traveltimes of the noisy far-offset traces can be more reliably picked to extend the useful aperture

of data. The first-arrival traveltimes of both the raw data after band-pass filtering and the super-virtual data are inverted to generate 2D velocity tomograms. The SVI tomogram reveals that the depth of penetration increased from 32 to 53 m after we included the far-offset traces and, hence, more details about the subsurface are shown.

One drawback of this method is that, due to the limited recording aperture and coarse spacing of the source and receivers, there will be artefacts in the super-virtual data set. In this case, a dip filter of the original data or a least-squares approach to the redatuming might be used to mitigate such noise. Another drawback is that improper windowing of the refraction arrivals can inadvertently lead to reconstructing far-offset refractions from shallow layers rather than deep layers.

REFERENCES

Bharadwaj P. and G.T. Schuster. 2010. Extending the aperture and increasing the signal-to-noise ratio of refraction surveys with super-virtual interferometry. AGU Annual Meeting Abstracts.

Bharadwaj P. and G.T. Schuster. 2012. Super-virtual refraction interferometry: Wide-angle OBS example: *Geophysical Journal International*, Submitted.

Bharadwaj P., Schuster G.T. and Mallinson I. 2011. Super-virtual refraction interferometry: Theory. *SEG Expanded Abstracts* **30**, 3809–3813.

Dong S., Sheng J. and Schuster G.T. 2006. Theory and practice of refraction interferometry. *SEG Expanded Abstracts*, 3021–3025.

Funck T., Andersen M.S., Neish J. and Dahl-Jensen T. 2008. A refraction seismic transect from the Faroe islands to the Hatton-Rockall Basin. *Journal of Geophysical Research* **113**, B12405.

Hanafy S.M. 2010. Locating of sinkhole extension by seismic refraction tomography and GPR methods. *EAGE Expanded Abstract*.

Higuera-Diaz C.P., Carpenter J. and Thompson M.D. 2007. Identification of buried sinkholes using refraction tomography at Ft. Campbell Army Airfield, Kentucky. *Environmental Geology* **53**, 805–812.

Mallinson I., Bharadwaj P., Schuster G.T. and Jakubowicz H. 2011. Enhanced refractor imaging by suwper-virtual inteferometry. *The Leading Edge* **30**, 546–550.

Mooney W.D. and Weaver C.S. 1989. Regional crustal structure and tectonics of the pacific coastal states: California, Oregon, and Washington: Geophysical framework of the continental United States. *Geological Society of America Memoir* **172**, 129–161.

Nichols J., Mikesell D. and Wijk K.V. 2010. Application of the virtual refraction to near-surface characterization at the boise hydrogeophysical research site. *Geophysical Prospecting* **58**, 1011–1022.

Schuster G.T. 2009. *Seismic Interferometry*. Cambridge University Press.

Sheriff R. and Geldart L. 1995. *Exploration Seismology*. Cambridge University Press.

Zelt C. and Smith R. 1992. Seismic traveltime inversion for 2-D crustal velocity structure. *Geophysical Journal International* **108**, 16–34.

Zhu X., Sixta D. and Angstam B. 1992. Tomostatics: Turning-ray tomography + static Corrections. *The Leading Edge* **11**, 15–23.